Catalysis Today 154 (2010) 271–282

Contents lists available at ScienceDirect

Catalysis Today

journal homepage: www.elsevier.com/locate/cattod

Fundamental understanding of deactivation and regeneration of cobalt Fischer–Tropsch synthesis catalysts

A.M. Saib[a,*], D.J. Moodley[a], I.M. Ciobîcă[b], M.M. Hauman[a], B.H. Sigwebela[a], C.J. Weststrate[c], J.W. Niemantsverdriet[c], J. van de Loosdrecht[a]

[a] Sasol Technology Pty (Ltd.), P.O. Box 1, Sasolburg 1947, South Africa
[b] Sasol Technology Netherlands B.V., Eindhoven University of Technology, P.O. Box 513, 5600 MB Eindhoven, The Netherlands
[c] Schuit Institute of Catalysis, Eindhoven University of Technology, P.O. Box 513, 5600 MB Eindhoven, The Netherlands

ARTICLE INFO

Article history:
Available online 15 March 2010

Keywords:
Gas-to-liquid
Cobalt
Fischer–Tropsch
Deactivation and regeneration

ABSTRACT

Cobalt-based Fischer–Tropsch synthesis (FTS) catalysts are an integral part of the gas-to-liquid (GTL) process. Due to the cost of both cobalt and noble metals, which are often used as promoters, an extended catalyst life is required to make the process economically feasible. Fundamental understanding of the deactivation mechanisms at play during FTS is key to extending catalyst lifetime. Most of the research on cobalt catalyst deactivation in the last 15 years has focused on oxidation as a deactivation mechanism. From our work it can be concluded that oxidation is not a deactivation mechanism during FTS for supported Co catalysts with crystallite size in excess of 2 nm. On the contrary the FT environment was found to be strongly reducing. Following a comprehensive study into the deactivation of a cobalt catalyst under realistic FTS conditions the following intrinsic deactivation mechanisms were identified: (1) sintering of Co active phase, (2) carbon deposition and (3) surface reconstruction. Having identified these mechanisms a three-step regeneration process, i.e.: (1) dewaxing (2) oxidation and (3) reduction, was tailored to reverse the sintering, carbon deposition and surface reconstruction that takes place during FTS.

1. General introduction

Supported cobalt catalysts are preferred for the Fischer–Tropsch synthesis (FTS) step in the gas-to-liquid (GTL) process due to its high activity and selectivity to linear paraffins. An alumina-supported cobalt catalyst is currently used in the commercial Sasol Slurry Phase Distillate™ (Sasol SPD™) process at Oryx in Qatar which is a joint Qatar Petroleum–Sasol GTL plant with a nominal capacity of 34,000 barrels per day and a capital investment of about $1 billion [1]. The construction of this plant was approved when the oil price was about $25/bbl. This GTL plant started up in 2007 and is currently running very well. Full design capacity was reached in 2009, using Sasol's proprietary alumina-supported cobalt-based FTS catalyst.

Supported cobalt-based catalysts are also employed in Shell's Middle Distillate Synthesis (SMDS) process at Bintulu, Malaysia, a GTL plant with a 14,700 barrels per day capacity using fixed bed reactors [2], and will be used in Shell's Pearl project in Qatar, which is under construction. In modern times, the use of cobalt as a FTS catalyst in coal-to-liquid (CTL) plants has not materialized commercially yet. Iron based catalysts are normally the preferred catalyst for CTL, due to the perceived risk that the synthesis gas quality (i.e. possible presence of catalyst poisons) is not suitable for cobalt catalysts. However, based on commercially available gas clean up systems and experience at Sasol on demonstration scale using coal derived synthesis gas for cobalt-based FTS runs, it is believed that in specific instances cobalt catalysts are very well suited for CTL ventures. This is in agreement with a recent announcement by Syntroleum that they have demonstrated the use of cobalt catalysts for coal-to-liquids [3]. Indeed, the first FTS catalyst applied for coal conversion by Ruhrchemie in Germany in the early 1930s was based on cobalt [4].

The FTS performance of cobalt catalysts is of course of utmost importance for the economics of the GTL process. The laboratory scale developed catalysts need to have sufficient productivity, which is a combination of a high activity (i.e. CO converted per mass of catalyst per unit time) and the correct selectivity (i.e. a high C_5^+ selectivity and a high α value, while keeping the CH_4 selectivity to a minimum).

In addition to having a high catalyst activity and selectivity, catalyst deactivation is an important topic for industrial catalyst development and is normally not studied extensively in the academic environment. In this paper, deactivation of cobalt-based FTS catalysts is studied as a change in catalyst activity as a function of

* Corresponding author. Tel.: +27 16 960 4263; fax: +27 11 522 4488.
E-mail address: Abdool.Saib@Sasol.com (A.M. Saib).

0920-5861/$ – see front matter © 2010 Elsevier B.V. All rights reserved.
doi:10.1016/j.cattod.2010.02.008

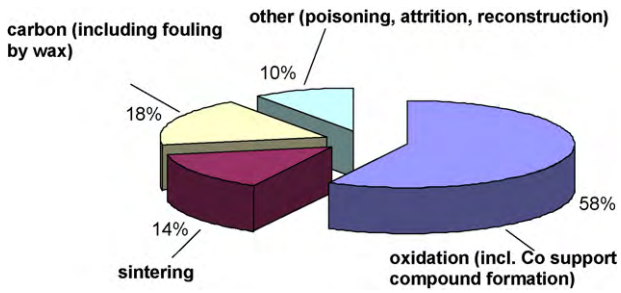

Fig. 1. Current focus areas of cobalt catalyst deactivation research (results of a SCOPUS search conducted on research articles from 1995 to 2009. Search terms are cobalt + Fischer–Tropsch + the relevant deactivation mechanism).

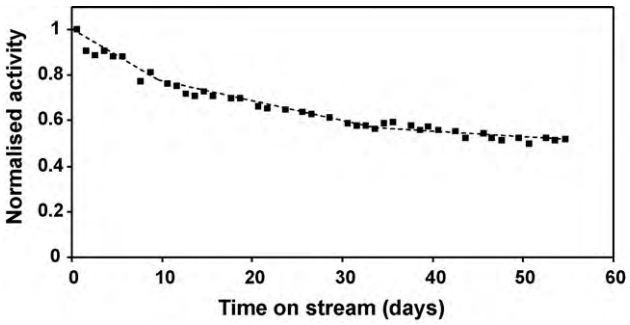

Fig. 2. Normalized activity for a $Co/Pt/Al_2O_3$ catalyst during realistic Fischer–Tropsch synthesis in a laboratory scale micro-slurry reactor at fixed CO conversion (adapted from [15]).

time on stream. Currently deactivation of cobalt catalysts is postulated to be due to a number of different deactivation mechanisms [5], such as (i) poisoning by sulphur and/or nitrogen containing compounds in the synthesis gas feed, which is especially important for CTL applications, (ii) oxidation of the active cobalt metal to an inactive cobalt oxide, (iii) cobalt-support compound formation like cobalt silicates and cobalt aluminates, (iv) sintering of small cobalt crystallites into larger ones, (v) surface reconstruction and (vi) carbon formation, and will be dealt with in Section 2.

It is interesting to note that many of the above deactivation mechanisms that plague modern cobalt catalysts were identified for the archetypical Co/ThO_2/Kieselguhr catalysts operating in the first commercial plants in Germany in 1930s [6]. Catalyst deterioration was ascribed to pore blockage by product wax, poisoning by lay-down of carbon deposits or sulphur and sintering of the active phase [6]. It is important to note that using the existing analytical tools available at that time there was no evidence for oxidation of the cobalt metal nor for metal-support compound (cobalt silicate) formation.

It is evident that most of the research on cobalt catalyst deactivation in the last 15 years has been focused on the oxidation as a major mechanism for activity loss. From a total of 133 papers mentioning cobalt catalyst deactivation, almost 60% dealt with the issue of oxidation (Fig. 1).

To extend the catalyst life, it is important to be able to regenerate a deactivated cobalt FTS catalyst and use it again in the FTS process. Although regeneration has been applied previously [7,8] the mechanism of regeneration is not completely clear. Section 3 in this paper deals with the recovery of the catalyst's FTS performance following regeneration, i.e. the reversal of the identified deactivation mechanisms and its fundamental understanding.

2. Catalyst deactivation

2.1. Catalyst activity profile and catalyst testing

To determine the Fischer–Tropsch synthesis (FTS) activity and deactivation of supported cobalt catalysts for commercial application, it is important to test the catalysts for extended periods under realistic FTS conditions [9]. In this study an alumina-supported cobalt catalyst promoted with platinum was tested in a slurry bubble column reactor with a diameter of 0.9 m using synthesis gas that was generated from natural gas by means of an auto thermal reformer (ATR). Clean synthesis gas was used ruling out significant deactivation due to poisons in the feed.

The catalyst used in these studies was a 20 wt% Co on alumina catalyst promoted with 0.5 wt% platinum and prepared by means of slurry phase impregnation, drying in vacuum, fluidized bed calcination at 250 °C, and fluidized bed reduction at 425 °C [10–14]. This resulted in a catalyst with cobalt crystallites with a population average of 6 nm as measured with transmission electron microscopy. This catalyst was tested at realistic FTS conditions (230 °C, 20 bar, H_2 + CO conversion of 50–70%, feed gas composition of 50–60 vol.% H_2 and 30–40 vol.% CO) and the FTS deactivation behaviour is shown in Fig. 2. It can be seen that the activity of the cobalt catalyst shows a decrease of about 40% during the first 30–40 days on stream, after which it starts levelling off [15]. This catalyst system is used to benchmark catalyst improvements investigated by Sasol. Improvements relative to this benchmark have already been commercially applied and others are in the development pipeline.

Representative slurry samples, containing a mixture of spent catalyst and Fischer–Tropsch synthesis wax, were taken directly from the demonstration reactor under a nitrogen blanket and were allowed to settle and congeal. The stability of these wax-coated catalyst samples against artificial oxidation in air was demonstrated previously [15] using XANES. This method thus allows for analysis of spent catalysts outside the reactor without changing the properties of the spent catalysts, and is referred to as pseudo-in situ. The resulting samples were characterized extensively to study the oxidation, carbon, sintering and regeneration behaviour as a function of catalyst age.

2.2. Poisoning by means of sulphur and nitrogen containing compounds

Sulphur poisoning of cobalt catalysts is well known and it is clearly an issue for cobalt-based FTS [16]. In a recent study Co catalysts were poisoned with ammonium sulphide during catalyst preparation, simulating a synthesis gas feed with 20 vppb sulphur containing compounds [17]. It was assumed that all sulphur from the ammonium sulphide adsorbed on the catalyst and has the same impact as sulphur coming from sulphur containing compounds in the real gas feed. The FTS results showed a clear impact of sulphur on the FTS activity, even when using sulphur levels as low as 20 vppb S.

In this paper, sulphur co-feeding experiments in a micro-slurry reactor using H_2S, COS and mercaptans on a 100–400 vppb level showed that sulphur has a negative impact on the activity of cobalt-based FTS catalysts (Fig. 3) [18]. The sulphur was adsorbed completely on the catalyst and a sulphur mass balance of about 90% could be achieved, by analysing sulphur in the gas feed, the tail gas and on the spent catalyst.

DFT simulations were performed for adsorbed sulphur on several sites on two close-packed cobalt surfaces, i.e. Co (111) and Co (0001) (Table 1). Sulphur has large adsorption energy at a low coverage and it is not surface or even site specific, meaning that sulphur has no clear preference for a particular cobalt site. However, due to its size and also to the electronic effect, sulphur will poison also the adjacent Co sites. Once adsorbed, sulphur is difficult to remove and it will accumulate with time, as stated also by Bartholomew [16,19]. Bulk cobalt sulphide, as well as subsur-

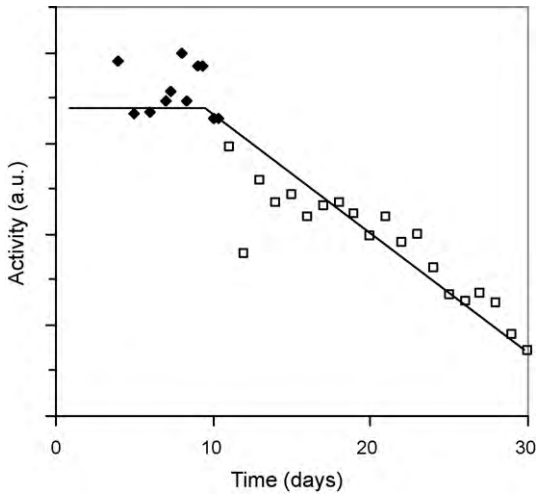

Fig. 3. Impact of sulphur co-feeding during FTS on the cobalt catalyst activity [14] (♦, clean feed; □, 190 vppb H_2S in feed).

face sulphur species does not form easily. This is supported by the energy needed to form subsurface sulphur ($S_{octa/fcc\text{-}Co}$ = 304 kJ/mol, $S_{octa/hcp\text{-}Co}$ = 196 kJ/mol).

Sulphur poisoning can however relatively easily be prevented by cleaning the synthesis gas feed properly, e.g. by using zinc-oxide or lead-oxide guard beds.

Poisoning of cobalt-based FTS catalysts by means of nitrogen containing compounds like NH_3 and HCN has been previously published [20–22]. It was shown that cobalt catalysts are rapidly but reversibly deactivated by HCN and NH_3 [20]. Syntroleum showed that cobalt catalysts can be deactivated by 16–38% (Extent), depending on the type and level of N containing poison ([22]; Table 2). The impact of nitrogen containing compounds is less than that of sulphur containing compounds, and it can be reversed with a mild hydrogen treatment. It is however worthwhile removing these nitrogen containing compounds to a vppb level [21]. The mechanism of poisoning by these nitrogen containing compounds is postulated to be competitive adsorption.

2.3. Oxidation of cobalt

As mentioned earlier, oxidation of the active cobalt metal phase to the inactive cobalt oxide phase during Fischer–Tropsch synthesis has been studied extensively in literature ([5] and references therein). Papers have been published that show oxidation is an issue; while others have claimed that oxidation does not occur during Fischer–Tropsch synthesis. It is clear that no consensus opinion existed until recently ([5] and references therein; [15,23–25]). Thermodynamic calculations have shown that oxidation of bulk cobalt to cobalt oxides (i.e. CoO or Co_3O_4) is not possible at industrial Fischer–Tropsch synthesis conditions (i.e. P_{H_2}/P_{H_2O} = 0.5–3.0) [26]. Cobalt aluminate formation is feasible from a thermodynamic point of view. This is however kinetically hindered at FTS relevant temperatures. Recent surface thermodynamic calculations, taking the surface energy contribution of cobalt metal and cobalt oxides into account, indicated that oxidation of small cobalt crystallites (<4.5 nm) is possible during Fischer–Tropsch synthesis [23].

Table 2
Activity loss data as caused by HCN and NH_3 (adapted from [22]).

Run	Temp (°C)	N species	N level (ppm)	Activity loss (% act/h)
A	210	NH_3	2.5	5.5
C	210	NH_3	1.0	0.9
E	215	HCN	0.3	0.7
F	217	HCN	3.0	13.9

A supported cobalt on alumina catalyst with cobalt metal crystallite of about 6 nm was used during realistic Fischer–Tropsch synthesis in a slurry bubble column reactor at realistic FTS conditions [15]. Wax covered spent catalyst samples were taken from the reactor and were used for catalyst characterization purposes. X-ray absorption near edge spectroscopy (XANES) measurements were performed on wax-coated samples, ensuring that the catalyst did not get oxidized during the XANES measurement. The XANES spectrum of the freshly reduced catalyst, after wax coating and prior to FTS, is a combination of the Co metal reference compound and CoO reference compound [15]. From the results of the spent catalyst samples, taken from the FTS reactor at different time intervals for a period of around 100 days, and using a linear combination of reference compounds the amount of cobalt metal in the different samples was calculated to increase with time on stream during FTS. Hence, to the contrary, the FTS environment is a strongly reducing environment. These results were supported by magnetic measurements and XRD analyses [5]. Based on the sensitivity of XANES it can thus be concluded that cobalt metal crystallites of 6 nm do not undergo surface or bulk oxidation during FTS under realistic conditions.

To further support this planar model catalyst were used to study the surface oxidation of cobalt particles [25]. Silica flat model cobalt catalysts were prepared by means of spin coating a cobalt solution on an oxidized SiO_2/Si(100) wafer. Cobalt crystallites with a size of 4–5 nm were obtained in this manner. In situ near edge x-ray absorption fine structure (NEXAFS) experiments were executed to study the surface oxidation behaviour of the model catalyst under model FTS conditions. The model conditions that were applied were P_{total} = 0.4 mbar, P_{H_2O}/P_{H_2} = 1, 150–400 °C. It was shown that the catalyst after reduction at 500 °C clearly portrays a cobalt metal spectrum. Exposure to the model H_2/H_2O conditions at temperatures from 150 to 450 °C did not cause any surface oxidation. When at 450 °C the hydrogen flow was stopped and only a water atmosphere was present, the cobalt surface started oxidizing and the spectrum is similar to that of the calcined catalyst. This clearly showed oxidation in a water atmosphere. The H_2/H_2O experiments convincingly showed that surface oxidation is not at play during FTS at these model conditions supporting the XANES measurements [25].

To get further evidence on surface oxidation, molecular modelling calculations were performed to study the stability of oxygen

Table 1
Adsorption energies (kJ/mol) of sulphur on cobalt surfaces from DFT calculations. fcc and hcp refer to the adsorption site and fcc and hcp refer to the Co structure: fcc is cubic or beta cobalt, while hcp is hexagonal or alpha cobalt (in-house results).

Coverage (%)	Shcp/fcc-Co(111)	Sfcc/fcc-Co(111)	Socta/fcc-Co(111)	Shcp/hcp-Co(0001)	Sfcc/hcp-Co(0001)	Socta/hcp-Co(0001)
11	−157			−161		
22	−139			−141		
25	−161	−166	304	−164	−162	196
33	−136			−132		
50	−87	−83		−87	−82	
75	−15	−12		−15	−12	

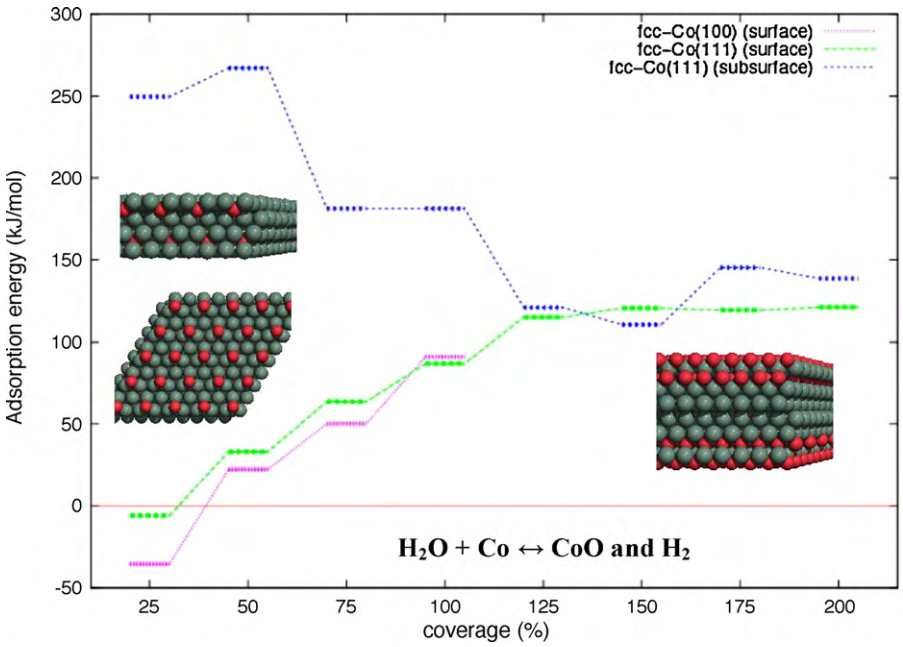

Fig. 4. Molecular modelling results for the dissociation of water on cobalt fcc surface (100) and (111) as well as subsurface oxygen on Co(111).

from water on the fcc-Co(111) and fcc-Co(100) surfaces as well as on fcc-Co(111) subsurface (Fig. 4). The equation used during the calculations was as follows: $H_2O + Co \leftrightarrow CoO$ and H_2. Water dissociation on the Co(100) is exothermic for a 25% oxygen coverage, i.e. 1 oxygen atom per 4 cobalt atoms. However, for higher coverages water dissociation becomes endothermic. Water dissociation on fcc-Co(111) is less favourable than on Co(100), and the pathway where oxygen goes subsurface after water dissociation is very endothermic. It could be argued that water dissociation on the more open (100) surface is more stable than on the more dense (111) surface, suggesting that surface roughness or crystallite size might play a role in the oxidation process. Surface oxidation via water dissociation will thus not occur for cobalt crystallites, and only small levels of oxygen will adsorb on the surface.

The above results have clearly shown that (surface) oxidation is not a deactivation mechanism during Fischer–Tropsch synthesis for the used catalyst systems.

In literature, however, some papers report oxidation as a deactivation mechanism, although others did not observe oxidation. Previously [5], we have shown that the oxidation of cobalt is dependant on the cobalt crystallite size and reactor water and hydrogen partial pressure ratios. We have updated this reconciliation (see Fig. 5) with revised thermodynamic calculations from Swart [27], who showed that the surface energy for cobalt oxide was previously [23] underestimated. Furthermore, data from literature that reported on the formation of cobalt–aluminate and/or cobalt–silicate were removed, as our renewed understanding is that these cobalt-support compounds are formed from unreduced cobalt oxide and not from cobalt metal that was oxidized (see cobalt-support formation Section 2.4). Recently published data from Bezemer et al. [28] and Elbashir et al. [29] were added. We have therefore come to the conclusion that (surface) oxidation under realistic FTS conditions does not occur for cobalt crystallites larger than 2 nm. This is supported by recent publications on this topic over the period 2003–2009 [5,15,23–25,28–31].

2.4. Cobalt-support formation

Although the formation of cobalt aluminate is kinetically hindered at FTS temperatures it may be accelerated due to the presence of product water. Water has been shown to increase the rate of metal aluminate formation [32] on model catalysts consisting of cobalt evaporated onto polycrystalline γ-alumina. Various authors [33–36] have also claimed that high water partial pressure increases the formation of aluminate on cobalt-based catalysts either during FTS or at model conditions in mixtures of H_2/H_2O. Often the observed deactivation is ascribed to the formation of aluminate as it is proposed that the irreducible cobalt-support species is formed from/at the expense of active metallic cobalt.

In a similar manner to the oxidation study wax-coated samples were removed periodically from the same extended slurry bubble column reactor run operated at realistic FTS conditions (see Section 2.1) and analysed with X-ray absorption near edge spectroscopy (XANES) [37]. It was clear from our measurements that during realistic FTS conditions the $Co/Pt/Al_2O_3$ catalyst undergoes reduction and ≤2–3 wt% cobalt aluminate formation takes place (Fig. 6). Based on the observation that the catalyst undergoes a relatively rapid reduction and a very gradual but slight cobalt aluminate formation it is proposed that this minor cobalt aluminate is formed from

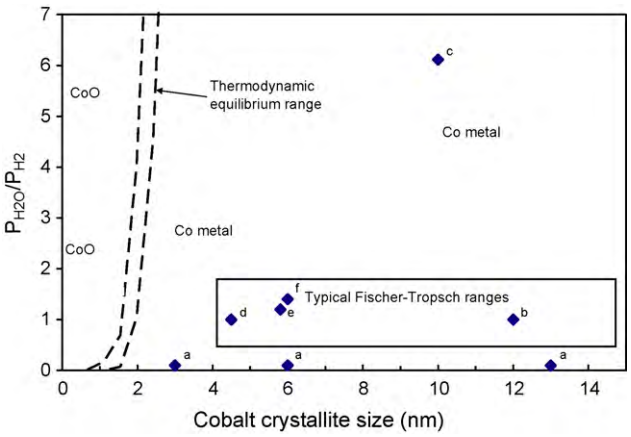

Fig. 5. Reconciliation of the effect of the water/hydrogen reactor ratio as a function of cobalt crystallite size on the oxidation behaviour of cobalt: (a) from [28]; (b) from [29]; (c) from [30]; (d) from [25]; (e) from [15]; (f) from [5]. All the data are superimposed on the thermodynamic equilibrium data range [27].

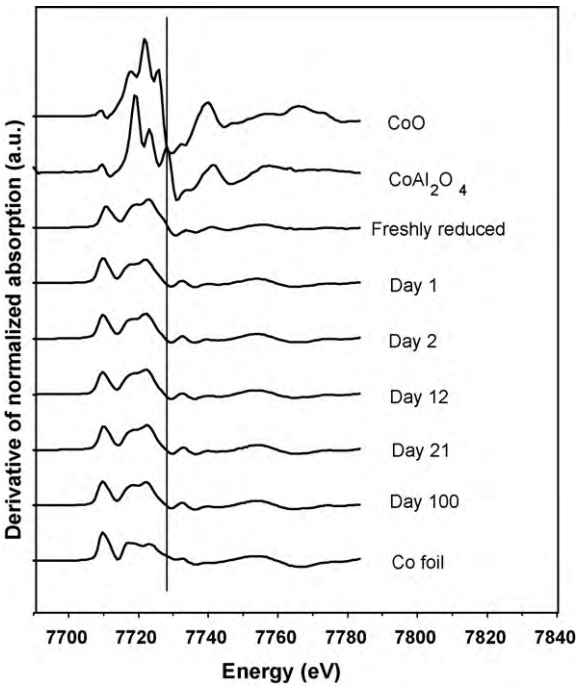

Fig. 6. XANES derivative spectra of $Co/Pt/Al_2O_3$ catalysts taken at different intervals from an extended FTS run, compared to reference compounds. Quantitative analysis of the XANES spectra using linear combination showed a maximum of around 3 wt% cobalt aluminate after 100 days of FTS [37].

the residual cobalt oxide present in the catalyst following reduction. To further support this we found that exposing the catalyst to higher water partial pressures (10 bar) during FTS in a lab-micro-slurry reactor increased the amount of cobalt aluminate formed, at the expense of CoO and not the metal, to around 10% [37]. Hence, the formation of cobalt aluminate during FTS does not necessarily imply oxidation of cobalt metal or deactivation. Using this knowledge Fig. 5 was updated to remove points where it was not clear if the support compound formation was from unreduced CoO or via the Co metal [5].

In terms of the mechanism, the formation of cobalt aluminate is known to proceed via CoO as an intermediate [7]. The presence of water can result in hydration of the alumina support as reported by Oukaci and coworkers [38]. The hydrated alumina appears to enhance the diffusion of small CoO particles in strong interaction with the support, during prolonged treatment resulting in the formation of non-reducible cobalt aluminate. This may explain why larger amounts of aluminate are formed in the case of catalyst exposed to higher water partial pressures.

Based on our observations we conclude that that cobalt aluminate formation does not significantly influence deactivation of cobalt catalysts during realistic FTS conditions.

2.5. Sintering

Sintering is a common deactivation mechanism for metal catalysts in all kinds of reactions. Sintering of cobalt-based FTS catalysts has however not been reported in literature very extensively. The group of Davis [39] has mentioned sintering of cobalt in spent Co/Al_2O_3 catalysts, and showed with extended x-ray absorption fine structure (EXAFS) that the coordination number for the first Co–Co shell of the metallic phase increased from 2.7 to 7.6 during FTS using a catalyst with cobalt crystallites of 5–6 nm. Bian et al. [30] showed sintering of cobalt crystallites from 10 to 17 nm and from 29 to 32 nm, for a Co/SiO_2 catalyst, during FTS at 240 °C, 10 bar and 90% conversion using hydrogen chemisorption. Sintering during FTS at 240 °C was much more pronounced than at 200 °C. Kiss et al. [40] observed for a Co/SiO_2 catalyst water induced sintering of cobalt crystallites from 5 to 11 nm, as measured with TEM, after FTS at 220 °C, 35 bar total pressure and 10 bar steam.

We have studied the aspect of sintering as a catalyst deactivation in detail [41] by analysing spent cobalt catalyst samples taken from the same extended slurry bubble column reactor run (see Section 2.1) at different time intervals.

Transmission electron microscopy (TEM) was performed using a high angle annular dark field (HAADF) detector on fresh/spent $Co/Pt/Al_2O_3$ catalyst samples that were microtomed. These TEM/HAADF images of the freshly reduced cobalt catalyst prior to FTS show small cobalt crystallite between 3 and 15 nm, with a maximum abundance of around 6 nm (i.e. an average surface area weighted size of 9.5 nm), which are located in larger grape-like regions of cobalt crystallites (Fig. 7). These grape-like features have dimensions of around 100 nm and are distributed widely over the alumina support. Comparing this TEM image of a fresh catalyst with a spent catalyst after 20 days of FTS, shows an increase in the cobalt crystallite size and a partial disappearance of the grape-like features (Fig. 7). By counting on the TEM images approximately 1000 cobalt crystallites per sample a cobalt crystallite size distribution can be obtained. This cobalt crystallite size distribution can be used to calculate an average cobalt crystallite size as a function of time on time during FTS (Fig. 8). It can clearly be seen that the crystallite size rapidly increases during the first few days of FTS where after it levels off. The area weighted average cobalt crystallite size, as determined by TEM, increases from about 9 nm for the fresh catalyst to about 15 nm of the spent catalyst.

From the increase in the area weighted average cobalt crystallite size with time on stream it was calculated, assuming a direct correlation between cobalt metal surface area and cobalt catalyst

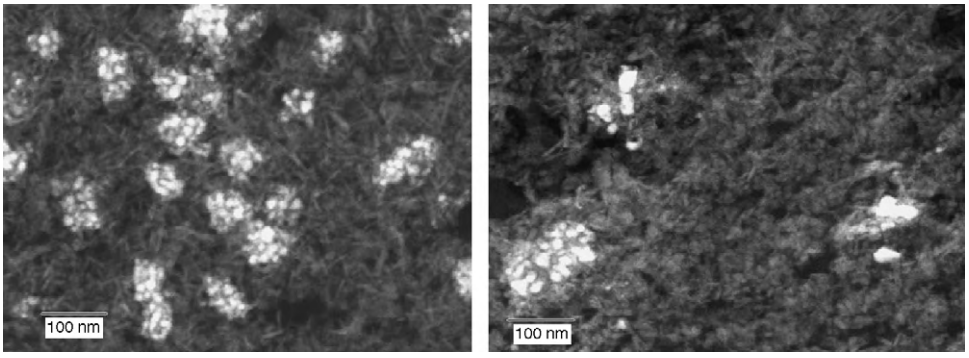

Fig. 7. HAADF–TEM images of a freshly reduced catalyst (left) and of a spent catalyst after 20 days of FTS in a demonstration unit (right) [15].

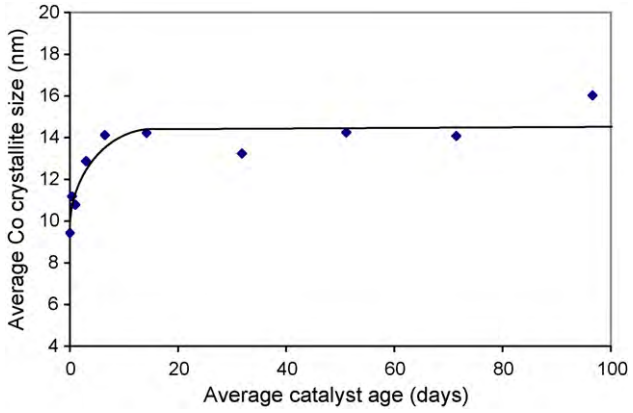

Fig. 8. Average surface area weighted cobalt crystallite size as function of average catalyst age, as determined by means of TEM/HAADF [41].

activity, that sintering can contribute to about 30% of the observed loss in activity [41].

2.6. Carbon formation

Carbon is present on cobalt FTS catalysts due to the dissociation of CO, which is considered an elementary step in the reaction [42]. This carbon is an intermediate specie which can be converted via hydrogenation and coupling to FTS products. The carbon may also be transformed to more stable species over time which may affect FTS activity [43]. It has been previously reported that both bulk cobalt carbide and polymeric carbon, if present can negatively influence FTS activity [43,44]

Carbon formation/deposition is a difficult deactivation mechanism to characterize on cobalt-based FTS catalysts [45]. This is due to the low quantities of carbon that are responsible for the deactivation (<0.5 mass%) coupled with the presence of wax that is produced during FTS. Furthermore, carbon is only detrimental to the FTS performance if it is bound irreversibly to an active site or interacts electronically with it. Hence, not all carbon detected will be responsible for deactivation, especially if the carbon is located on the support.

Recently, we undertook a study on carbon deposition of cobalt-based catalysts [45] by analysing spent cobalt catalyst samples taken from the same extended slurry bubble column reactor run (see Section 2.1) at different time intervals. The catalyst samples were wax extracted with tetrahydrofuran (THF) under argon at mild conditions (around 65 °C) and transferred into a glove box in a protected environment, for passivation. In order to follow the accumulation and reactivity of the carbon on the passivated catalysts, a combination of temperature programmed hydrogenation (TPH) and temperature programmed hydrogenation/oxidation (TPH/TPO) was used. TPH of the used catalysts showed the presence of three broad types of carbonaceous species (Fig. 9). The least reactive species toward hydrogen (peak 3, ~430 °C) was identified as polymeric carbon based on previous literature [46] and measurements of reference carburized compounds [45]. Coupled TPH/TPO experiments were performed to remove the less reactive carbon species and showed an increase in the polymeric type of carbon with TOS in amounts that were significant to block the available cobalt surface (Fig. 10).

As mentioned earlier, the location of the inert polymeric carbon is believed to be a key issue in determining its effect on catalyst activity. Using a combination of hydrogen chemisorption, carbon and cobalt mapping with energy-filtered transmission electron microscopy (EFTEM), and low-energy ion scattering (LEIS), we were able to determine that the polymeric carbon was located on both

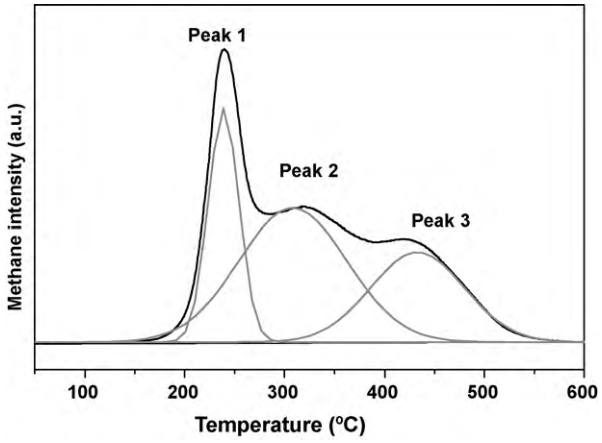

Fig. 9. Peak deconvolution of a methane profile for TPH of a wax-extracted $Co/Pt/Al_2O_3$ catalysts from the FTS run in the slurry bubble column. Peak 3 was identified as a polymeric type of carbon (from [45]). Reprinted from [45], with permission from Elsevier.

cobalt and the alumina support [45]. The polymeric carbon located on the cobalt was postulated as one of the causes of activity decline in the extended FTS run. Indeed, regeneration of the catalyst to remove the polymeric carbon resulted in a dramatic recovery in the FTS activity [45] (see also Section 3.4).

2.7. Carbon oligomers (as precursors of polymeric carbon)

Under hydrogen depleted conditions the formation of CH_x during FTS is reduced and atomic carbon can simply couple together resulting into small carbon oligomers [27,47]. It also possible that over time active surface carbon is gradually transformed to more stable oligomeric species under standard FTS conditions [45]. Coupling reactions of atomic carbon atoms on a fcc-Co(111) surface were studied using theoretical methods. It was found that oligomeric species are energetically more stable compared with the individual atoms. Once formed the carbon fragments can couple together forming large carbon agglomerates known commonly as polymeric carbon or can form more regular structures such as graphene. These structures if formed may result in loss of catalyst activity due to geometric blocking and provide a plausible explanation for the observed increase in polymeric carbon on catalysts tested at realistic conditions, seen in the previous section. See Fig. 11 for a graphical illustration of some carbon oligomers [47].

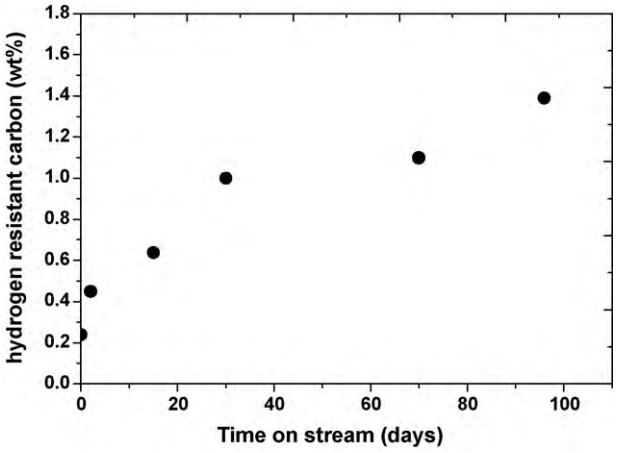

Fig. 10. Polymeric carbon amounts obtained from TPO experiments following TPH which represents carbon resistant to hydrogen at 350 °C (adapted from [45]).

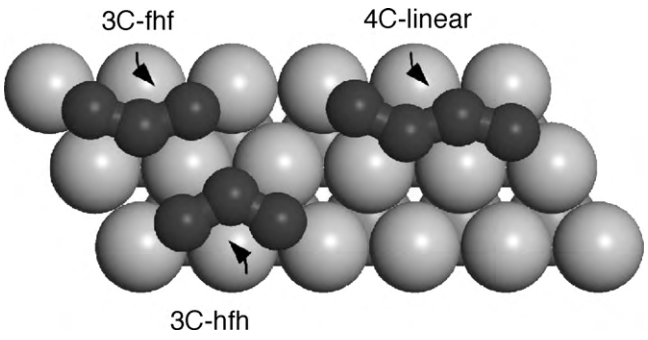

Fig. 11. An example of few small carbon oligomers on fcc-Co(111). Trimers (3C-fhf: two carbon atoms on fcc sites and one on hcp site in between; 3C-hfh: two carbon atoms on hcp sites and one on fcc site in between) and 4 carbon linear tetramer shown (from [47]). Reprinted with permission from [47], Copyright 2008 American Chemical Society.

The stability of the carbon oligomers increases with the number of carbon atoms up to about 4, after which it becomes constant. A further increase of stability is obtained when a 6 member ring is formed. Upon increasing the size the oligomer will bind to the surface only with the terminal carbon atoms.

2.8. Subsurface carbon

Burghgraef [48] studied the relative stability of subsurface carbon on Co and Ni clusters. His findings were that atomic carbon will enter the metal lattice and the structure will be stable. In-house calculations have shown that for a large range of coverages, atomic carbon will adsorb subsurface with adsorption energies comparable of the surface sites. This is in agreement with other reported work [49] that shows that diffusion of carbon into the first subsurface layer is thermodynamically favourable and the corresponding activation energy is low. The most common subsurface adsorption site is the octahedral site, where carbon atom will have three metal atoms neighbours from the surface and three metal atoms neighbours from the second layer. The octahedral site is located just under the fcc adsorption site. Two tetrahedral subsurface sites are possible as well, but they are much higher in energy. They are located one under the hcp adsorption site and one under the top site. At 25% coverage of atomic carbon on fcc-Co(111) the octahedral subsurface site is only 1 kJ/mol less stable than the most stable surface site, which is the hcp three-fold site. Increasing the coverage usually results in mixed combinations with some carbon atoms lying subsurface and some lying on the surface. The presence of surface polymeric carbon on the catalysts as seen in Section 2.6 thus implies that it is plausible that subsurface carbon is also present during FTS conditions.

Theoretical calculations on the conversion of surface carbide to subsurface carbon on hcp-Co(0001) found that the electron withdrawing power, and therefore the poisoning effect on potential CO adsorption, is maximal for subsurface carbon [50]. In the presence of subsurface carbon, metal d_{xz} orbitals are less likely to accept electrons from the CO 5σ orbital, and thus metal–CO bonding will weaken. The d_{xz} orbital will in turn be less able to back-donate into the CO 2π orbital, resulting in additional metal–CO bond weakening as well as reduced C–O bond weakening. The net result is that the presence of subsurface carbon is likely to reduce both CO adsorption and dissociation processes on nearby atoms. Experimental work has also linked the presence of subsurface carbon to catalyst deactivation [49].

2.9. Carbon-induced surface reconstruction

It has been observed that cobalt surfaces may undergo large-scale reconstruction under a synthesis gas environment [51]. Reconstruction is a thermodynamically driven process that results in the formation of more stable surfaces with a structure that is different from the bulk-terminated surface structure. Recently Bezemer et al. [28] found with in situ X-ray adsorption spectroscopy (XAS) that the average coordination number of small carbon-supported Co particles (<6 nm) decreases during FTS. This was interpreted as reconstruction and flattening of the Co particles, which can result in decreased activity. Conversely, CO induced restructuring is mentioned by Schulz et al. [52] as an activation mechanism of cobalt FTS catalysts.

Molecular modelling work performed in this study on fcc cobalt (100) showed that a coverage of 50% atomic carbon will induce

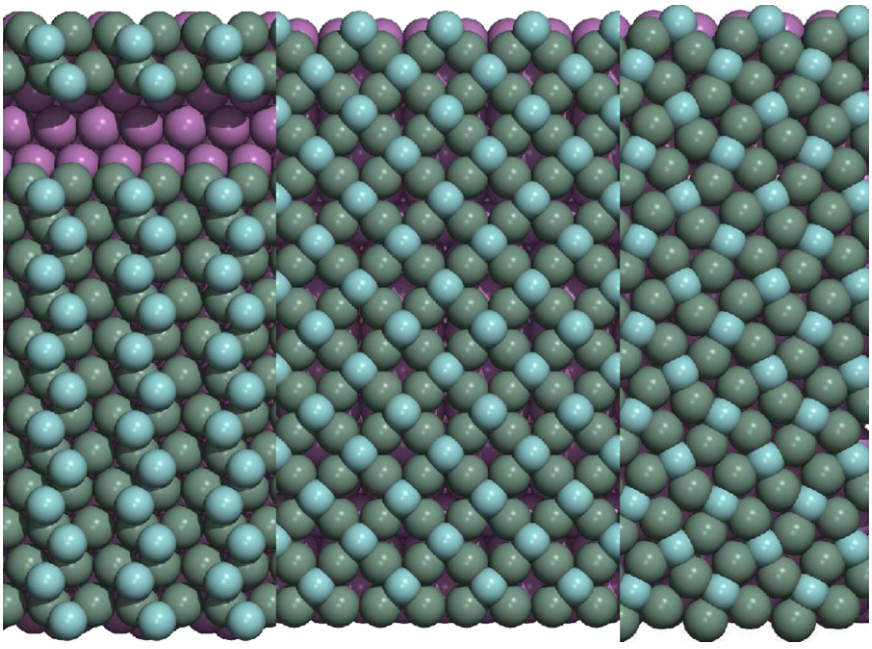

Fig. 12. Left: the unreconstructed surface of 50% C/fcc-Co(111) with the same density of surface atoms as fcc-Co(100). Center: carbon induced (111) to (100) surface reconstruction. Right: the clock reconstructed surface of 50% C/fcc-Co(100)/fcc-Co(111). Reprinted from [53], with permission from Elsevier.

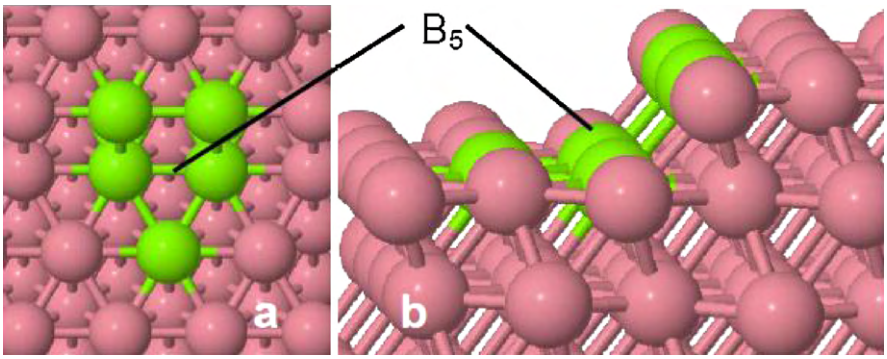

Fig. 13. Top (a) and side (b) view of the penta-coordinated B5 site which occurs at the step where (100) and (111) planes intersect.

a clock type reconstruction similar to that observed for the classic case of Ni(100) [53]. The adsorption energy of the carbon is stabilized by 15 kJ/mol compared to the unreconstructed surface, resulting in a more stable surface [53]. The reconstruction results in a shorter distance between the carbon and cobalt but also an increase in coordination of the cobalt atoms, and thus fewer broken bonds. The barrier for the carbon-induced clock reconstruction was found to be very small (1 kJ/mol), which suggested that the process is not kinetically hindered. Interestingly, of all the absorbates studied (B, N, O, CO, C, CH and CH_2) it was found that only atomic carbon could induce this reconstruction indicating that CO dissociation is required for such a reconstruction.

Also fcc-Co(111) was found to reconstruct in the presence of adsorbed atomic carbon. A similar clock reconstruction of Ni(111) surface was reported earlier [54]. The reconstruction is easier to understand if one decomposes it into two parts. Firstly a reconstruction from fcc-Co(111) to fcc-Co(100), followed by a clock reconstruction of the resulting fcc-Co(100) layer. Since the second is very similar to the above reconstruction, we focus on the first one. Due to the difference in the density of surface atoms it is better to compare the surface energies rather than the adsorption energies. A 50% carbon coverage on a 100 layer on top of a 111 slab is 56 kJ/mol more stable than having a 50% carbon coverage on a 111 slab. This was calculated on a 14×2 unit cell (due to the lattice mismatch) see Fig. 12.

Again, from the list of intermediates (C, O, CH_2, CO) only atomic carbon is able to induce such a reconstruction. Hence, during FTS carbon deposition can take place which in turn could drive surface reconstruction and cause deactivation. This reconstruction may also result in deactivation due to shape changes in the cobalt particle.

Conversely the reconstruction of cobalt could also assist in the formation of the active sites for FTS as proposed by Wilson and de Groot [51], i.e. a C7 site. From our work [55] we propose that during restructuring additional B5 sites are produced which are the active sites for FTS and are known to dissociate CO a lot easier than other surface sites.

Active B5 sites are composed of a three-fold site adjacent to a four-fold site, sharing two metal atoms and having an angle larger than 90, but smaller than 180, as one can see from Fig. 13. Restructuring the surface of a metal particle often results in a surface with different surface atoms density which means that step surfaces will be created and additional B5 sites could be formed.

2.10. Deactivation overview

The above sections have been summarized in Table 3 and it can be seen that only sintering, carbon deposition and surface reconstruction are important deactivation mechanisms for clean synthesis gas.

3. Catalyst regeneration

This section deals with the reversal of the identified deactivation mechanisms and understanding of this reversal.

3.1. Experimental

3.1.1. Regeneration procedure

The spent wax protected catalyst from the FT run (ca. 56-day-old sample: see Section 2.1) was subjected to the following oxidative regeneration treatment to reverse the primary deactivation mechanisms.

The spent catalyst was solvent washed with heptane at 100 °C to remove excess wax.

The catalyst sample was subsequently subjected to a calcination (i.e. oxidation) step in a fluidized bed calcination unit, using an air/N_2 mixture and the following heating program: 2 °C/min to 300 °C, 6–8 h hold at 300 °C. The oxygen concentration was gradually increased from 3 to 21% O_2/N_2 to control the exotherm. The oxidized catalyst sample was subsequently subjected to a reduction in pure hydrogen in a fluidised bed unit using the following heating program: 1 °C/min to 425 °C, 15 h hold at 425 °C. The reduced catalyst was off loaded into wax.

3.1.2. TEM analyses of regenerated catalyst

The regenerated catalyst following reduction was passivated with dry ice. The passivated catalyst samples were set in resin and

Table 3
Deactivation mechanisms along with their importance and severity.

Mechanism	Severity	Importance	Comment
Poisoning sulphur	High	Not important	Can be removed from syngas
Poisoning HCN/NH_3	Medium	Not important	Can be removed from syngas
Oxidation	None	Not important	Not observed
Metal–support interaction	None	Not important	Formed from unreduced CoO
Sintering	High	Important	Can cause 30% decrease in activity
Carbon deposition	High	Important	Gradual deposition of largely polymeric carbon with TOS
Surface reconstruction	Medium	Possibly important	Is induced by carbon and may also play a role in genesis of the B5 site

microtomes (<100 μm) prepared. A Philips CM200 TEM with a LaB_6 filament as electron source was used for the analysis. This instrument is operated at 200 kV. High angle annular dark field (HAADF) images were obtained in nanoprobe STEM mode using a Fischione detector.

3.1.3. Temperature programmed hydrogenation/oxidation (TPH/TPO) coupled with mass spectroscopic (MS) measurements

In each TP-MS experiment a 100 mg sample of the wax-extracted catalyst was loaded into a quartz reactor (4 mm internal diameter). In coupled TPH/TPO experiments, the wax-extracted catalysts were first treated in flowing He for 30 min before ramping the temperature in a 50% He/H_2 mixture (20 ml/min) to 350 °C at 10 °C/min and holding there for 1 h. The reactor was then cooled to room temperature, flushed with He for 30 min and then heated to 900 °C at 10 °C/min in 10% O_2/He flow of 20 ml/min and held there for 1 h. The evolution of CO_2 ($m/z = 44$) as a gasification product of carbon ($C + O_2 \rightarrow CO_2$) was monitored. For direct TPO measurements the hydrogenation step above was eliminated.

3.1.4. XRD analyses of regenerated catalyst

XRD analysis was performed in a Panalytical X'Pert Pro MPD diffractometer on samples that were removed at different stages of the oxidation step. Phase identification was done using X'Pert Highscore Plus and quantitative Rietveld refinement was done using Topas and the fundamental parameter approach.

3.1.5. FTS testing of regenerated catalyst in continuously stirred reactor (CSTR)

The regenerated catalyst was tested in a lab CSTR to determine its FTS activity. Fifteen grams of reduced catalyst and paraffin wax (200 g) were loaded into the reactor, heated to 230 °C and subjected to FTS by flowing syngas (50–60 vol.% H_2 and 30–40 vol.% CO) through the reactor, which was set to 20 bar total pressure.

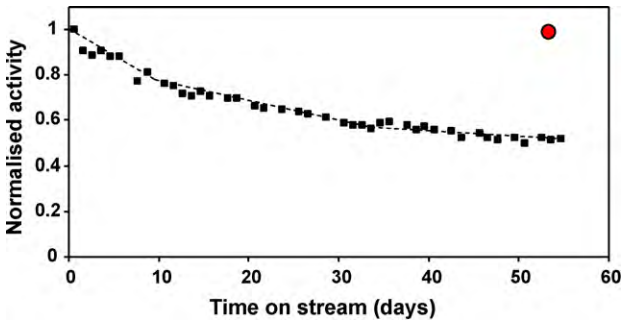

Fig. 14. (a) Normalized activity for a $Co/Pt/Al_2O_3$ catalyst during realistic Fischer–Tropsch synthesis in a demonstration scale slurry reactor and (b) spent sample subject to ex situ oxidative regeneration (closed circle).

Argon (10 vol.% of the feed gas) was added as an internal standard. The syngas conversion was determined by GC-TCD analysis and was maintained at 60–63%.

3.1.6. Flat model catalyst preparation

Details about the flat model system that was used to study catalyst morphology changes during oxidation–reduction can be found elsewhere ([56] and references therein). In brief, it consists of a ~10 nm thick Si_3N_4 layer, which is terminated by a SiO_2 layer on the outside. The cobalt active phase was deposited by spincoating an aqueous solution of cobalt nitrate. A polymer (polymethylvinylether) was added to the solution to increase its viscosity. After deposition the sample was calcined at 350 °C (3 h, 20% O_2 in Ar), which proved to be sufficient to remove the polymer (measured using X-ray photoelectron spectroscopy). After calcination the sample was reduced at 425 °C (3 h, pure H_2), and passivated at room temperature by controlled exposure to oxygen. The experimental conditions during further calcination and reduction treatments were the same. TEM analysis was performed at

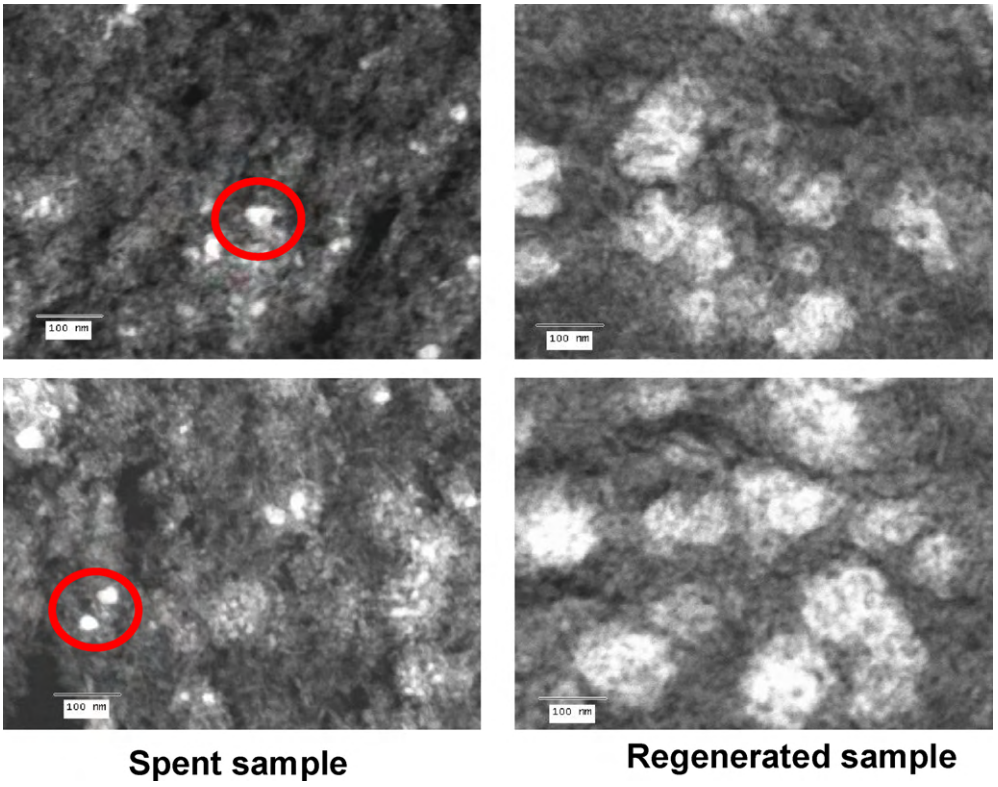

Fig. 15. TEM analyses of the 56-day spent FT catalyst as compared to the same catalyst following regeneration, i.e. oxidation, reduction and passivation.

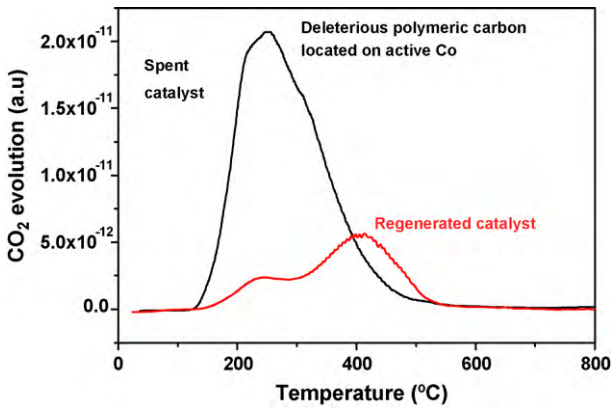

Fig. 16. TPO analyses of a 56-day-old spent catalyst following hydrogenation at 350 °C as compared to the same sample following regeneration (adapted from [45]).

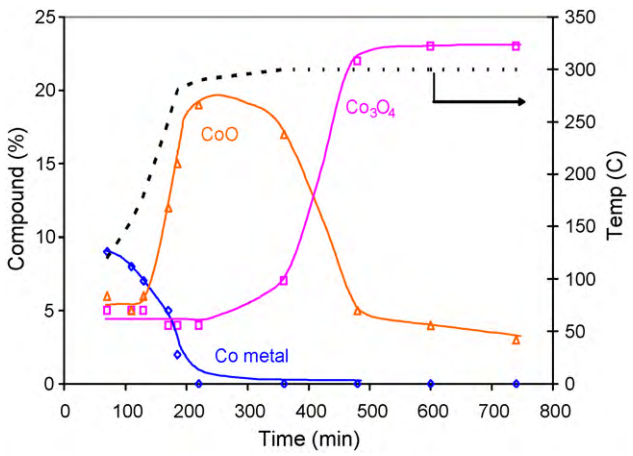

Fig. 17. XRD phase analyses of regenerated catalyst at different stages of oxidation.

room temperature using a FEI Tecnai G2 Sphera electron microscope, operated at 200 kV.

3.2. Activity recovery upon regeneration

To reverse the primary deactivation mechanisms, i.e. sintering and carbon deposition, an oxidative regeneration treatment was applied to the catalyst (see Section 3.1.1). Fig. 14 shows that following oxidative regeneration the spent catalyst recovered its activity completely to that of the fresh catalyst. To understand the reasons for the recovery in activity the regenerated catalyst was characterized and compared to the spent catalyst.

3.3. TEM analyses of regenerated and spent catalyst

Fig. 15 shows the TEM analyses of the 56-day spent FT catalyst as compared to the same catalyst following regeneration. The images of the spent catalyst show some large cobalt crystallites, while after regeneration the grape-like features containing smaller cobalt crystallites are again visible It is thus clear from Fig. 15 that the Co crystallites in the spent catalyst undergoes a redispersion following regeneration which would contribute to the recovery of the spent FT catalyst following regeneration.

3.4. Temperature programmed oxidation (TPO) analyses of spent and regenerated sample

Fig. 16 shows TPO analyses of a spent 56-day-old sample following solvent wash and TPH to 350 °C as compared to the same sample following regeneration. From Section 2.6 it was shown that part of the polymeric carbon left over following hydrogenation at 350 °C was present on the cobalt surface and contributes to the deactivation of the catalyst during FTS. Fig. 16 shows that the regeneration procedure is able to remove a large part of the polymeric carbon that is responsible for deactivation. It is also clear that some of the carbon undergoes transformation during the oxidation step and can only be removed in air at temperatures is excess of 350 °C. The atomic carbon responsible for surface reconstruction would also be reversed by the oxidation treatment.

3.5. XRD analyses of regenerated catalyst at different stages of oxidation

XRD phase analyses were performed on catalyst samples that were removed at different stages of the oxidation process. Fig. 17 shows the phases analyses for the catalyst as a function of time on stream during oxidation. It is clear that as the oxidation proceeds the Co metal is transformed to CoO and then to Co_3O_4. At relatively low temperatures the Co metal starts being oxidized to CoO, while the oxidation of CoO to Co_3O_4 only starts at about 300 °C after CoO reaches a maximum. At the end all Co metal has disappeared and mainly Co_3O_4 is present.

3.6. Flat model work

The use of transparent, flat model supports offers the advantage that the Co nanoparticles can be imaged with an excellent contrast. It is also possible to return to the same particles on the sample, so morphology changes after oxidation and reduction treatments can be studied on the level of the individual particle. This approach was used to study the morphology changes that occur during calcination of a metallic catalyst and also the reduction of the calcined sample. This process thus simulates the regeneration process steps. The result of this approach is shown

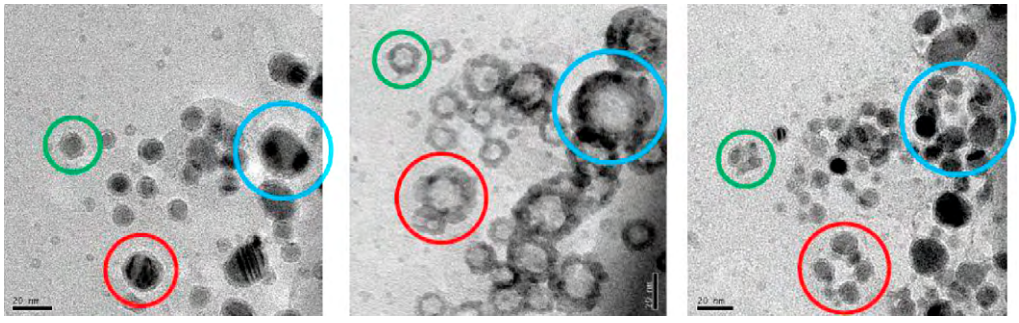

Fig. 18. Co particles supported on a flat SiO_2 support during different stages of an oxidation–reduction cycle. Model catalyst in the metallic state before oxidation (left). Hollow oxide particles, formed upon oxidation (middle). Reduction of the hollow particles, which break up into several smaller metallic particles (right).

in Fig. 18. The morphology at the start of the series is shown on the left-hand side: the support is covered with metallic Co particles (as confirmed by electron diffraction) with a variety of particle sizes. The ~3 nm thick passivation layer of CoO (chemical nature confirmed by XPS) is visible as a shell around the metallic core. The central picture shows the same sample area after calcination. The metallic particles have transformed into hollow oxide particles (Co_3O_4), with a much larger outer diameter than the original metal particle [57]. This phenomenon has been observed previously during reaction of nanoparticles. In the case of cobalt nanoparticles void formation has been reported for reaction of Co with sulphur, selenium and oxygen [57,58]. At the basis of this lies the Kirkendall effect [59,60]. The Kirkendall effect is a consequence of the different diffusivities of cobalt and oxygen. Rapid outward diffusion of Co through the oxide layer creates lattice defects, which condensate into "Kirkendall voids" close to the metal–oxide interface. In this way the oxidation mechanism leads to transport of cobalt away from its original location. During reduction (right-hand image) the hollow oxide particles break up into a number of smaller particles, located at the position of the original oxide shell. When the image before and after the oxidation–reduction cycle is compared it is clear that the cobalt phase is redispersed, i.e. large particles have broken up into smaller ones.

3.7. Regeneration overview

To summarize, the oxidative regeneration procedure is able to reverse the major deactivation mechanism, i.e. sintering, carbon deposition and surface reconstruction. Based on literature [61,21] the current regeneration procedure will not be able to reverse sulphur poisoning but will reverse NH_3/HCN poisoning. The latter can be removed with a simple hydrogen treatment [21].

4. General discussion and conclusions

Fundamental understanding of catalyst deactivation is key to designing more stable catalysts that can be regenerated. Catalyst deactivation is a thermodynamically driven process and is inevitable for most catalysts. The main deactivation mechanisms of cobalt catalysts from literature are: (i) poisoning by sulphur and/or nitrogen containing compounds in the synthesis gas feed, which is especially important for CTL applications, (ii) oxidation of the active cobalt metal to an inactive cobalt oxide, (iii) cobalt-support compound formation like cobalt silicates and cobalt aluminates, (iv) sintering of small cobalt crystallites into larger ones (v) surface reconstruction and (vi) carbon formation.

Most of the research on cobalt catalyst deactivation in the last 15 years has focused on oxidation as a deactivation mechanism for activity loss. From a total of 133 papers mentioning cobalt catalyst deactivation, almost 60% dealt with the issue of oxidation (Fig. 1). From our work using a host of techniques (NEXAFS, XANES, magnetic measurements, XRD, computational chemistry) it can be concluded that surface or bulk oxidation is not a deactivation mechanism during FTS for supported Co catalysts with crystallite size in excess of 2 nm. In fact it was clearly shown by us [15] that the FT environment is strongly reducing and further reduction of the unreduced CoO takes place. This finding is corroborated by work on both alumina-supported [29] and model cobalt systems [62,63]. The XANES analyses also showed that a minor amount of cobalt aluminate was formed during FTS. As oxidation of Co does not take place it was concluded that the source of the cobalt aluminate is the unreduced CoO in the fresh catalyst implying that cobalt aluminate formation does not contribute to deactivation. In summary the unreduced CoO in the fresh catalyst reacts by means of reduction and cobalt aluminate formation. Based on this conclusion data in literature where it is stated that cobalt aluminate contributes to deactivation should be treated cautiously.

Sintering is clearly present during FTS and can contribute to up to 30% of deactivation. The mechanism of sintering is not clear at this stage and appears to be related to the reduction of cobalt. Sintering and further reduction of the catalyst appears to dominate the deactivation at early stages of the reaction whereas polymeric carbon deposition is responsible for the long-term deactivation. In-house calculations have shown that carbon oligomer formation is favourable. These oligomers are the precursors to polymeric carbon. Our theoretical work has shown that surface carbon and subsurface carbon are equally favourable from an energetic point of view and it is expected that subsurface carbon will exist on cobalt during FTS. Previous theoretical [47] and experimental work [46] has shown that subsurface carbon will electronically influence CO adsorption and dissociation and could possibly have a detrimental effect on catalyst activity.

In addition to surface blockage the high coverage of atomic carbon also contributes to surface reconstruction which is a thermodynamically driven process and may result in deactivation due to shape changes in the cobalt particle. From DFT calculations it was shown that C will drive reconstruction. On the contrary it appears from literature that the FTS surface also undergoes reconstruction to form the active phase, i.e. step sites. Our work indicates that the B5 site is the active site for FTS [55]. The formation of the active site during FTS and the contribution of reconstruction to deactivation need further work.

The above deactivation mechanisms, i.e. sintering, carbon deposition and surface reconstruction are intrinsic to cobalt and we believe will be present on most Co based FTS catalysts.

Based on the fundamental understanding of the deactivation mechanisms an oxidative regeneration procedure was developed to reverse the deleterious carbon deposition and sintering that takes place during FTS. TPO measurements on the spent catalyst showed that a large part of the carbon that is located on the Co can be removed between 200 and 350 °C. A mild oxidation at 300 °C was sufficient to remove most of the deleterious carbon. Interestingly Fig. 16 shows that a part of the polymeric carbon (peak at 350 °C) is transformed into a harder to remove carbon. This could be reduced to some extent by increasing the oxidation temperature however excessive oxidation >400 °C will result in $CoAl_2O_4$ formation. During the oxidation treatment the spent catalyst which contains largely Co metal undergoes a phase change to CoO and then Co_3O_4. The initial stages of oxidation are dominated by Co to CoO formation and thereafter CO_2 formation and CoO to Co_3O_4 transition proceeds in parallel. TEM analyses showed that the re-reduction of the oxidized catalyst leads to a redispersion of Co. Using a $Co/SiO_2/Si(100)$ flat model system a plausible mechanism of redispersion was identified. It was shown that oxidation of Co metal leads to hollow sphere formation by the Kirkendall effect. The hollow sphere formation results in a spreading of the Co which then undergoes multi-nucleation during reduction resulting in smaller Co crystallites. Hence, both the oxidation and reduction are key to the reversal of sintering, i.e. redispersion. A model catalyst was used due to the complexity of the industrial catalyst which results in inferior TEM images. Hence, the oxidation–reduction cycle results in a redispersion of Co and a removal of the deleterious carbon which restores the activity of the spent catalyst.

5. Conclusions

Following a comprehensive study into the deactivation of a cobalt catalyst under realistic FTS conditions the following deactivation mechanisms were identified: (1) sintering of Co active phase, (2) carbon deposition and (3) surface reconstruction. These deac-

tivation mechanisms are intrinsic to cobalt and will be present on most Co based FTS catalysts. Fundamental understanding of these deactivation mechanisms with respect to the active site, i.e. B5 site, is key to improving catalyst stability.

Having identified these mechanisms a three-step regeneration process, i.e.: (1) dewaxing (2) oxidation and (3) reduction, was tailored to reverse the sintering, carbon deposition and surface reconstruction that takes place during FTS. This oxidative regeneration process successfully restored the FTS performance of the spent catalyst to that of the fresh catalyst.

Acknowledgements

The authors acknowledge Esna du Plessis for XRD measurements and Willem Erasmus for HAADF–TEM measurements.

References

[1] A.P. Steynberg, M.E. Dry, Fischer–Tropsch technology, Stud. Surf. Sci. Catal. 152 (2004) 441.
[2] M.M.G. Senden, A.D. Punt, A. Hoek, Stud. Surf. Sci. Catal. 199 (1998) 943, http://www.shell.com/home/content/aboutshell/our_strategy/major_projects_2/pearl/overview/.
[3] Syntroleum, http://www.syntroleum.com, 20 November 2007.
[4] B. Cornils, W.A. Herrmann, M. Rasch, Angew. Chem. Int. Ed. 33 (1994) 2144.
[5] J. van de Loosdrecht, B. Balzhinimaev, J.-A. Dalmon, J.W. Niemantsverdriet, S.V. Tsybulya, A.M. Saib, P.J. van Berge, J.L. Visagie, Catal. Today 123 (2007) 293.
[6] British Intelligence Objectives Sub-committee. Interrogation of Dr Otto Roelen of Ruhrchemie A.G., B.I.O.S.—Final report no 447; Item no 30 (1945) (http://www.fischer-tropsch.org).
[7] M.J. van der Burgt, J. Ansorge, GB 2,222,531, 1988 (Shell).
[8] R. Huang, K.L. Agee, B.A. Arcuri, P.F. Schubert, US 6,812,179 B2, US2002/0183403 A1; WO 02/085508 (Syntroleum).
[9] P.J. van Berge, S. Barradas, J. van de Loosdrecht, J.L. Visagie, Erdol Erdgas Kohle 117 (3) (2001) 138.
[10] R.L. Espinoza, J.L. Visagie, P.J. van Berge, F.H. Bolder, EP 0 736 326 B1 (1996).
[11] P.J. van Berge, J. van de Loosdrecht, E.A. Caricato, S. Barradas, US 6,638,889 B1 (1998).
[12] P.J. van Berge, J. van de Loosdrecht, E.A. Caricato, S. Barradas, B.H. Sigwebela, EP 1 119 411 B1 (1998).
[13] P.J. van Berge, J. van de Loosdrecht, J.L. Visagie, US 6,806,226 B2 (1999).
[14] P.J. van Berge, J. van de Loosdrecht, J.L. Visagie, T.J. van der Walt, H. Veltman, C. Sollie, EP 1 444 040 B1 (2001).
[15] A.M. Saib, A. Borgna, J. van de Loosdrecht, P.J. van Berge, J.W. Niemantsverdriet, Appl. Catal. A: Gen. 312 (2006) 12.
[16] C.H. Bartholomew, Appl. Catal. A: Gen. 212 (2001) 17–60.
[17] C.G. Visconti, L. Lietti, P. Forzatti, R. Zennaro, Appl. Catal. A: Gen. 330 (2007) 49–56.
[18] T.J. van der Walt, P.S. Nkwanyana, B.H. Sigwebela, J. van de Loosdrecht, E.L. Viljoen, Oral presentation, Catalysis Society of South Africa (CATSA), Cape Town, South Africa, 10–13 November, 2002.
[19] C.H. Bartholomew, R.M. Bowman, Appl. Catal. 15 (1985) 59–67.
[20] P.J. van Berge, E.A. Caricato, Oral presentation at Catalysis Society of South Africa (CATSA), Kruger National Park, South Africa, 5–8 November, 2000.
[21] S.C. Leviness, C.J. Mart, W.C. Behrmann, S.J. Hsia, D.R. Neskora, US 6,284,807 B1 (2001).
[22] J. Inga, P. Kennedy, S. Leviness, WO 2005/071044 (2005).
[23] E. van Steen, M. Claeys, M.E. Dry, J. van de Loosdrecht, E.L. Viljoen, J.L. Visagie, J. Phys. Chem. B 109 (2005) 3577–3757.
[24] A.M. Saib, A. Borgna, J. van de Loosdrecht, P.J. van Berge, J.W. Geus, J.W. Niemantsverdriet, J. Catal. 239 (2006) 326.
[25] A.M. Saib, A. Borgna, J. van de Loosdrecht, P.J. van Berge, J.W. Niemantsverdriet, J. Phys. Chem. B 110 (2006) 8657.
[26] P.J. van Berge, J. van de Loosdrecht, S. Barradas, A.M. van der Kraan, Catal. Today 58 (2000) 321.
[27] J. Swart, PhD thesis, UCT, Cape Town, South Africa (2008).
[28] G.L. Bezemer, J.H. Bitter, H.P.C.E. Kuipers, H. Oosterbeek, J.E. Holewijn, X. Xu, F. Kapteijn, A.J. van Dillen, K.P. de Jong, J. Am. Chem. Soc. 128 (2006) 3956.
[29] N.O. Elbashir, P. Dutta, A. Manivannan, M.S. Seehra, C.B. Roberts, Appl. Catal. A: Gen. 285 (2005) 169–180.
[30] G.-Z. Bian, N. Fujishita, T. Mochizuki, W.-S. Ning, M. Yamada, Appl. Catal. A: Gen. 252 (2003) 251.
[31] M. Ronning, et al., Combined XRD and XANES studies of a Re-promoted Co/gamma Al_2O_3 catalyst at Fischer–Tropsch synthesis conditions. Catal. Today (2009), doi:10.1016/j.cattod.2009.10.010.
[32] P.H. Bolt, "Transition metal–aluminate formation in alumina-supported model catalysts", PhD thesis, University of Utrecht, The Netherlands (1994).
[33] J. Li, G. Jacobs, T. Das, B.H. Davis, Appl. Catal. A 228 (2002) 203.
[34] D. Schanke, A.M. Hilmen, E. Bergene, K. Kinnari, E. Rytter, E. Ådnanes, A. Holmen, Catal. Lett. 345 (1995) 269.
[35] G. Jacobs, T.K. Das, P.M. Patterson, J. Li, L. Sanchez, B.H. Davis, Appl. Catal. A 247 (2003) 335.
[36] G. Jacobs, P.M. Patterson, Y. Zhang, T. Das, J. Li, B. Davis, Appl. Catal. A 233 (2002) 215.
[37] D.J. Moodley, "On the Deactivation of cobalt-based Fischer–Tropsch synthesis catalysts," PhD Thesis, Eindhoven University of Technology, The Netherlands (2008).
[38] A. Sirijaruphana, A. Horvath, J.G. Goodwin Jr., R. Oukaci, Catal. Lett. 91 (2003) 89.
[39] T.K. Das, G. Jacobs, P.M. Patterson, W.A. Conner, J. Li, B.H. Davis, Fuel 82 (2003) 805.
[40] G. Kiss, C.E. Kliewer, G.J. DeMartin, C.C. Culross, J.E. Baumgartner, J. Catal. 217 (2003) 127.
[41] M.J. Overett, B. Breedt, E. du Plessis, W. Erasmus, J. van de, Loosdrecht, Prepr. Pap. Am. Chem. Soc., Div. Petr. Chem. 53 (2) (2008) 126–128.
[42] D.J. Moodley, J. van de Loosdrecht, A.M. Saib, J.W. Niemantsverdriet, in: B.H. Davis, M.L. Occelli (Eds.), Advances in Fischer–Tropsch Synthesis, Catalysts, and Catalysis, CRC Press, 2009, p. 49.
[43] V. Gruver, R. Young, J. Engman, H.J. Robota, Prepr. Pap. Am. Chem. Soc., Div. Pet. Chem. 50 (2005) 164.
[44] V. Gruver, X. Zhan, J. Engman, H.J. Robota, Prepr. Pap. Am. Chem. Soc., Div. Pet. Chem. 49 (2004) 192.
[45] D.J. Moodley, J. van de Loosdrecht, A.M. Saib, M.J. Overett, A.K. Datye, J.W. Niemantsverdriet, Appl. Catal. A 354 (2009) 102.
[46] D.-K. Lee, J.-H. Lee, S.-K. Ihm, Appl. Catal. 36 (1988) 199.
[47] J.C.W. Swart, I.M. Ciobîcă, R.A. van Santen, E. Van Steen, J. Phys. Chem. C 112 (2008) 12899.
[48] H. Burghgraef, A quantum chemical study of CH and CC bond activation on transition metals, PhD thesis, Eindhoven University of Technology, The Netherlands (1995).
[49] J. Xu, K.F. Tan, A. Borgna, M. Saeys, First principles based promoter design for heterogeneous catalysis, in: Poster 476ae, AIChE Annual Meeting, San Francisco, 15 November, 2006, http://www.aiche.confex.com/aiche/2006/techprogram/S2113.htm.
[50] M.C. Zonneville, J.J.C. Geerlings, R.A. van Santen, Surf. Sci. 240 (1990) 253.
[51] J. Wilson, C. de Groot, J. Phys. Chem. B 99 (1995) 7860.
[52] H. Schulz, Z. Nie, F. Ousmanov, Catal. Today 71 (2001) 351.
[53] I.M. Ciobîcă, R.A. van Santen, P.J. van Berge, J. van de Loosdrecht, Surf. Sci. 602 (2008) 17.
[54] C. Klink, I. Stensgaard, F. Besenbacher, E. Lægsgaard, Surf. Sci. 360 (1996) 171.
[55] I.M. Ciobîcă, R.A. van Santen, J. Chem. Phys. B 107 (2003) 3808–3812.
[56] P.C. Thüne, J.W. Niemantsverdriet, Surf. Sci. 603 (2008) 1756–1762.
[57] Y. Yin, R.M. Rioux, C.K. Erdonmez, S. Hughes, G.A. Somorjai, A.P. Alivisatos, Science 304 (2004) 711–714.
[58] P.A. Chernavskii, G.V. Pankina, V.I. Zaikovskii, N.V. Peskov, P. Afanasiev, J. Phys. Chem. C 112 (2008) 9573–9578.
[59] H.J. Fan, U. Gösele, M. Zacharias, Small 3 (2007) 1660–1671.
[60] H.J. Fan, M. Knez, R. Scholz, D. Hesse, K. Nielsch, M. Zacharias, U. Gösele, Nanoletter 7 (2007) 993–997.
[61] A.L. Lapidus, M.A. Daage, A. Miche, R.J. Koveal, A.J. Krylova, A.B. Erofeev, US 6,455,596 (2001) (Exxon).
[62] H. Oosterbeek, Phys. Chem. Chem. Phys. 9 (2007) 3570.
[63] Z. Yan, Z. Wang, D.B. Bukur, D.W. Goodman, J. Catal 268 (2009) 196.